DALTON
FULL PAPER

Cyclo-[Ni(μ_2-SPh)$_2$]$_9$ and *cyclo*-[Ni(μ_2-SPh)$_2$]$_{11}$: new oligomeric types of toroidal nickel(II) thiolates containing geometrically unprecedented 9- and 11-membered ring systems †

Sergei A. Ivanov, Michael A. Kozee, W. Alex Merrill,‡ Sorabh Agarwal ‡ and Lawrence F. Dahl *

Department of Chemistry, University of Wisconsin-Madison, Madison, WI 53706, USA

Received 2nd May 2002, Accepted 15th August 2002
First published as an Advance Article on the web 10th October 2002

Two new oligomeric types of toroidal nickel(II) monothiolate ring systems, *cyclo*-[Ni(SPh)$_2$]$_{11}$ (**1**) and *cyclo*-[Ni(SPh)$_2$]$_9$ (**2**), containing heretofore unknown 11-membered ($n = 11$) and 9-membered ($n = 9$) ring-geometries, respectively, are reported. Our initial isolation of **1** was as an unexpected by-product that resulted from unsuccessful attempts to produce crystalline nanostructural gold thiolate clusters from reactions of alkyl/phenyl thiols with the recently prepared nanostructural $[Au_{16}Ni_{24}(CO)_{40}]^{4-}$ cluster. The unique architecture of **1** led to a designed preparation of it by a direct synthetic route involving reactions of PhSNa with Ni(ClO_4)$_2$ in THF or DMF. Slow addition of the reactants at low temperature afforded two crystal forms of **1**: namely, the previously isolated triclinic crystals ($P\bar{1}$) as well as solvated monoclinic crystals ($C2/c$) (**1a**). Normal mixing of the reactants at room temperature gave rise to a trigonal crystal form ($P\bar{3}12/c$) that was determined to be *cyclo*-[Ni(SPh)$_2$]$_9$ (**2**). The atomic arrangements and stoichiometries of both **1** and **2** were unequivocally established from low-temperature CCD area-detector X-ray diffractometry studies; particularly noteworthy is that the structures of both crystal forms of **1** possess nearly identical molecular geometries (including the phenyl-ring orientations) along with an encapsulated THF molecule. These new air-stable molecular additions to the *cyclo*-[Ni(μ_2-SR)$_2$]$_n$ family (with $n = 4$, 5, 6, and 8) are of particular stereochemical interest in that: (1) in sharp contrast to the previously known monodentate thiolate-bridged members which *ideally* possess *regular convex* Ni–S toroids, the assembled *n*-localized edge-fused square-planar [NiS$_4$] subunits found in the triclinic and monoclinic crystal forms of undecanickel **1** and in the trigonal crystal form of nonanickel **2** have irregularly-shaped mixed concave/convex toroidal pseudo-C_{2v} and pseudo-D_{3h} ring geometries, respectively, that are geometrically unique; (2) **1** is the first host member of any known *cyclo*-[Ni(SR)$_2$]$_n$ oligomer to have a co-crystallized solvated guest molecule (*viz.*, THF); and (3) the observed orientations of adjacent phenyl rings attached to the highly pyramidal sulfur atoms in both **1** and **2** suggest the occurrence of weakly attractive pairwise phenyl ··· phenyl dispersion forces that are presumed to stabilize these novel nickel(II) phenylthiolate oligomers. A comparative analysis of the salient solid-state structural features of the *idealized* Ni–S ring geometries of the resulting entire *cyclo*-[Ni(SPh)$_2$]$_n$ family ($n = 4$, 5, 6, 8, 9, and 11) is presented (under the assumed absence of sterically crowded R-substituents and/or abnormal packing effects). The unsymmetrical enlargement of the pseudo-threefold 9-membered ring in **2** by the formal insertion of two adjacent [Ni(SPh)$_2$] units to give an otherwise analogous Ni–S framework of the 11-membered ring in **1** is attributed to the elongated template-geometry of the guest molecule coupled with the maintenance of attractive pairwise phenyl ring interactions.

Introduction

Prior to 1965 nickel thiolates had been reported as insoluble high polymers.[1] The first structurally determined example of a soluble cyclic homoleptic nickel(II) thiolate ring-system was [Ni(μ_2-SEt)$_2$]$_6$.[2,3] Since that time, a considerable number of other geometrically similar cyclic [Ni(SR)$_2$]$_6$ ring-systems {with R = Me,[4] *n*-Pr,[5] $(CH_2)_2OH$,[6] $(CH_2)_2SiMe_3$,[7] $CH_2C_6H_4$(*p*-Cl),[8] $(CH_2)_3NMe_2$,[9] and $(CH_2)_3NMe_2H^+$[10]} that likewise contain sulfur-bridged nickel hexagons and two palladium analogues, [Pd(SR)$_2$]$_6$ {with R = $(CH_2)_2Me$[11] and $(CH_2)_2OH$[6]} have been prepared and structurally characterized. Concurrently, this resulting family of toroidal nickel(II) thiolates was greatly expanded to include three different types of polygonal series consisting of: (1) [Ni(SR)$_2$]$_4$ {with R = C_5H_9NMe,[12] C_6H_{11},[13] and *i*-Pr[14]} containing sulfur-bridged nickel tetragons (squares); (2) [Ni(SR)$_2$]$_5$ {with R = Et,[13] $(CH_2)_2N(i\text{-}Pr)_2$,[15] and CH_2SiMe_3[16]} containing sulfur-bridged nickel pentagons; and (3) one [Ni(SR)$_2$]$_8$ {with R = CH_2CO_2Et[17]} containing a sulfur-bridged nickel octagon. The first known nickel-selenium toroid, [Ni(Se(*i*-Pr))$_2$]$_4$ which is isostructural with the corresponding thiolate [Ni(S(*i*-Pr))$_2$]$_4$,[14] was recently reported.[18]

The nickel–sulfur architecture of each member of these four series of cyclic [Ni(SR)$_2$]$_n$ ($n = 4$, 5, 6, and 8) may be *ideally* viewed as a *regular convex n*-polygon of coplanar nickel atoms with two monothiolate sulfur atoms bridging each pair of adjacent nickel atoms such that each Ni(II) is coordinated to an approximate square-planar (*i.e.*, more precisely rectangular–planar) arrangement of four sulfur atoms. The resulting upper and lower parallel polygons of coplanar nonbonding sulfur atoms, which form a prismatic polyhedron, are in a staggered conformation with the *n*-polygonal Ni atoms; this parallel three-layer S/Ni/S sandwich was originally denoted as a *tiara*.[2] The *idealized* nickel–sulfur geometry may be best envisioned as *n* localized square-planar [NiS$_4$] subunits that are edge-fused on opposite nonbonding S ··· S edges to give an *n*-polygon

† Dedicated to Professor Ed Abel and Dr. Peter Woodward for highly insipiring research during their illustrious academic careers that included the preparation and structural analysis of the first tiara-like member, [Ni(μ_2-SEt)$_2$]$_6$, of the currently extensive oligomeric *cyclo*-[Ni(SR)$_2$]$_n$ family ($n = 4$, 5, 6, 8, 9, 11).
‡ Undergraduate research scholar.

DOI: 10.1039/b204273h

of nickel atoms. The R substituents of the monodentate thiolate ligands were found to be sterically disposed in alternating axial and equatorial positions about the *n*-polygonal nickel toroids in order to minimize steric interactions of the ligands; however, complete alternation is not possible for odd-membered polygonal nickel atoms (*i.e.*, $n = 5$). In the case of the octagonal $[Ni(SCH_2CO_2Et)_2]_8$, one of the axial substituents is bent inward such that its ethyl tail almost fills the toroidal cavity.[17]

Reported herein are the salient structural features of two remarkable new additions, $[Ni(SPh)_2]_{11}$ and $[Ni(SPh)_2]_9$, to this toroidal nickel(II) thiolate family. Their air-stable molecular architectures are of prime stereochemical interest for several reasons: (1) All previous reported cyclic $[Ni(\mu_2\text{-}SR)]_n$ *ideally* possess *regular convex* nickel–sulfur toroids, whereas the undecanickel **1** and nonanickel **2** have geometrically unprecedented mixed *convex*/*concave* nickel–sulfur toroids; (2) **1** is the first host member ($n = 11$) of the entire $[Ni(SR)_2]_n$ family to have a co-crystallized solvated guest molecule. Previous efforts to trap co-crystallized inclusion species within the *tiara* for the first established family member ($n = 6$, $R = C_2H_5$[2]) and later for the one octagonal member ($n = 8$[17]) were unsuccessful; (3) Dance *et al.*[17] stated that "larger toroids (than the octagonal member) are unlikely to form unless there is a central occupant, either a guest molecule or reentrant ligand (as found for $n = 8$), which by weak coordination to the metal, or by van der Waals interactions, provides some mechanical assistance"; and (4) From a subsequent theoretical investigation in 1993 of the bonding in the known toroidal nickel thiolates ($n = 4$, 5, 6, and 8), Alemany and Hoffmann[19] concluded that direct Ni(II) ··· Ni(II) and S ··· S interactions are not important factors (except, possibly, for $n = 4$) and that formation of strongly bound host–guest complexes is unlikely for nickel thiolate toroids.

Our research was motivated by the current intense interest in thiolate-stabilized Au nanoclusters, which have been isolated in nearly monodispersed sizes.[20] Consequently, we recently carried out reactions designed to obtain monodispersed, thiolate-stabilized $Au_{16}(SR)_x$ nanoclusters by reacting different alkyl/aryl thiols with the recently prepared bimetallic nanosized $[Au_{16}Ni_{24}(CO)_{40}]^{4-}$ tetraanion, for which its $Au_{16}Ni_{24}$ core-geometry is the first example of a microscopic ccp chunk of quasi-gold metal stabilized by close-packed carbonyl-ligated nickel layers.[21] Although our attempts to acquire crystalline gold thiolate nanoclusters were unsuccessful, the reaction with phenylmercaptan led to the isolation of a small quantity of crystals that were structurally determined to be **1**. Its existence then energized our desire to prepare this remarkable host molecular compound with an encapsulated THF guest from a *direct* synthetic route: for example, from the reaction of $Ni(ClO_4)_2$ (which is soluble in THF) with NaSPh in THF solution. However, the initial reaction involving a normal mixing of the reactants at room temperature provided trigonal crystals that instead were shown from an X-ray crystallographic investigation to possess another new type of nickel thiolate oligomer, *cyclo*-$[Ni(SPh)_2]_9$. Subsequent reactions performed at 0 °C involving a dropwise addition of NaSPh to $Ni(ClO_4)_2$ in THF solution gave (along with an insoluble precipitate) two different crystal forms of **1**. X-Ray diffraction studies of both forms revealed that we had achieved our goal in obtaining $[Ni(SPh)_2]_{11}$ by a simple preparative pathway. The majority of crystals were triclinic with unit-cell parameters that were essentially identical with those of the previously determined $[Ni(SPh)_2]_{11}\cdot 5THF$. The other crystal form was determined from a complete structural determination to be a solvated monoclinic phase of $[Ni(SPh)_2]_{11}$ (**1a**), but nevertheless having a closely related molecular geometry (*i.e.*, all phenyl rings were similarly disposed about the 11-membered nickel–sulfur ring) along with an encapsulated (two-fold disordered) THF molecule. Both the atomic arrangements and stoichiometries of **1** in the triclinic and monoclinic crystal phases (C_1 and C_2 site symmetry, respectively) and of **2** in the trigonal crystal phase (D_3 site symmetry) were unambiguously established from relatively precise low-temperature CCD X-ray diffractometry data.

Herein are presented the details of this research, including: (1) a comparison of the small but distinct variations in the molecular geometries of **1** and **1a** together with an analysis of their closely related packing modes in the triclinic and monoclinic crystal phases; (2) a comparison of the mean molecular parameters of **1** and **2** with each other and with those of the other types of *cyclo*-$[Ni(SR)_2]_n$ toroids (n = 4, 5, 6, and 8) containing monodentate thiolate R substituents; and (3) an hypothesis accounting for the self-assembly of the unprecedented geometries of both **1** and **2**.

Results and discussion

Structural features of the Ni–S architecture in the triclinic crystal form of *cyclo*-$[Ni(SPh)_2]_{11}$ (1)

The nickel–sulfur framework of *cyclo*-$[Ni(SPh)_2]_{11}$ (**1**) is shown in Fig. 1 and the molecular geometry in Fig. 2. Table 1 presents relevant molecular parameters. The top view in Fig. 1 of the cyclic $Ni_{11}S_{22}$ architecture discloses a highly deformed toroidal geometry of pseudo-C_{2v} symmetry formed *via* edge-fusions of 11 $[NiS_4]$ units at opposite nonbonding S ··· S edges. One mirror is comprised of the 11 approximately planar Ni atoms, the other mirror passes through one Ni and two bridging sulfur atoms, and the twofold axis is directed along the line of intersection of these two perpendicular mirrors. The resulting convex/concave-like toroid may be analyzed by use of a

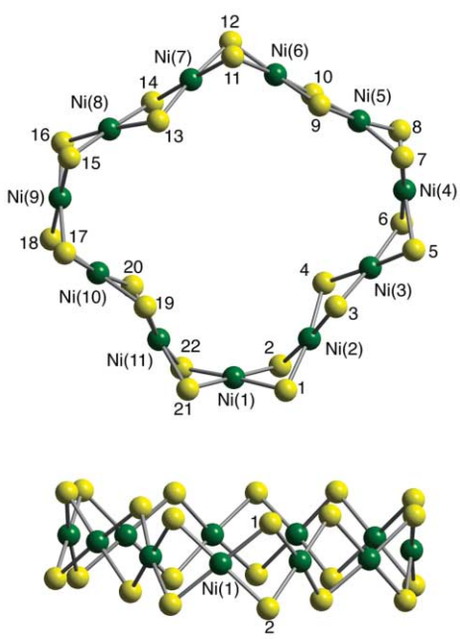

Fig. 1 Top and side views of the undecagonal nickel–sulfur framework in $[Ni(\mu_2\text{-}SPh)_2]_{11}$ (**1**). The top view ideally shows that edge-fusion of the 11 localized planar $[NiS_4]$ subunits along opposite nonbonding S–S edges gives rise to a highly irregular convex/concave-shaped triple-layer toroidal geometry that approximately conforms to pseudo-C_{2v} symmetry. One vertical mirror passes through Ni(1) and the two bridging S(11) and S(12) that connect Ni(6) and Ni(7); the other orthogonal vertical mirror contains the 11 essentially planar Ni atoms. These two perpendicular mirror planes define the 2-fold axis (along their line of intersection) that passes through Ni(1). The side view shows the virtually planar nonbonding Ni_{11} ring sandwiched between the two approximately coplanar nonbonding S_{11} rings. The diameter of the resulting four-leaf clover-shaped cavity varies from 8.8 to 11.7 Å. The two longer, nearly perpendicular distances of 11.5 and 11.7 Å are between the midpoint of S(11) and S(12) and the opposite Ni(1) and between the two opposite Ni(4) and Ni(9), respectively; the two shorter, nearly perpendicular distances of 8.8 and 9.1 Å are each between the midpoints of sulfur atoms in oppositely directed sulfur-bridging pairs.

Table 1 Mean molecular parameters under pseudo-C_{2v} symmetry of the Ni–S framework in *cyclo*-$[Ni(SPh)_2]_{11}$ for the triclinic (**1**) and monoclinic (**1a**) crystal forms and corresponding ranges for **1** [a]

A. Bonding and non-bonding distances

Connectivity [b]	N [c]	Mean/Å	Range/Å
Ni(1)–S(1)	4	2.215 (2.208)	2.207(6)–2.224(6)
Ni(2)–S(1)	4	2.203 (2.209)	2.194(6)–2.217(5)
Ni(2)–S(3)	4	2.207 (2.197)	2.200(5)–2.211(5)
Ni(3)–S(3)	4	2.204 (2.196)	2.197(5)–2.209(6)
Ni(3)–S(5)	4	2.219 (2.207)	2.196(5)–2.236(6)
Ni(4)–S(5)	4	2.219 (2.207)	2.200(6)–2.228(5)
Ni(4)–S(7)	4	2.215 (2.206)	2.207(6)–2.228(5)
Ni(5)–S(7)	4	2.218 (2.211)	2.209(5)–2.224(6)
Ni(5)–S(9)	4	2.209 (2.203)	2.200(5)–2.221(5)
Ni(6)–S(9)	4	2.200 (2.191)	2.179(6)–2.221(5)
Ni(6)–S(11)	4	2.210 (2.205)	2.210(5)–2.217(5)
		Av [d] 2.211 (2.204)	
Ni(1) ··· Ni(2)	2	2.90 (2.96)	2.894(3)–2.896(3)
Ni(2) ··· Ni(3)	2	3.19 (3.21)	3.186(3)–3.203(3)
Ni(3) ··· Ni(4)	2	2.93 (2.87)	2.919(3)–2.942(3)
Ni(4) ··· Ni(5)	2	2.91 (2.87)	2.897(3)–2.931(3)
Ni(5) ··· Ni(6)	2	3.26 (3.22)	3.237(3)–3.274(3)
Ni(6) ··· Ni(6′)	1	2.86 (2.83)	2.865(4)
		Av [d] 3.02 (2.99)	
S(1) ··· S(2)	2	2.92 (2.94)	2.917(9)–2.918(9)
S(3) ··· S(4)	2	2.90 (2.87)	2.897(9)–2.903(9)
S(5) ··· S(6)	2	2.94 (2.90)	2.936(9)–2.938(9)
S(7) ··· S(8)	2	2.95 (2.91)	2.954(9)–2.955(9)
S(9) ··· S(10)	2	2.94 (2.92)	2.918(9)–2.952(9)
S(11) ··· S(12)	1	2.77 (2.78)	2.766(11)
		Av [d] 2.92 (2.89)	
S(1) ··· S(3)	2	3.31 (3.32)	3.248(9)–3.373(9)
S(3) ··· S(5)	2	3.32 (3.32)	3.275(9)–3.399(9)
S(5) ··· S(7)	2	3.31 (3.32)	3.294(9)–3.323(9)
S(7) ··· S(9)	2	3.31 (3.31)	3.244(9)–3.389(9)
S(9) ··· S(11)	2	3.36 (3.35)	3.324(9)–3.390(9)
S(1) ··· S(1′)	1	3.33 (3.30)	3.333(9)–3.336(9)
		Av [d] 3.32 (3.32)	

B. Dihedral angles

δ/° [e]	N [c]	Mean/°	Range/°
Ni(1)S_2Ni(2)	2	121 (128)	121(1)–122(1)
Ni(2)S_2Ni(3)	2	213 (210)	211(1)–213(1)
Ni(3)S_2Ni(4)	2	124 (119)	123(1)–124(1)
Ni(4)S_2Ni(5)	2	124 (120)	122(1)–125(1)
Ni(5)S_2Ni(6)	2	194 (203)	186(1)–202(1)
Ni(6)S_2Ni(6′)	1	113 (111)	113(1)

C. Perpendicular displacement of Ni(i) from its mean sulfur plane in each $[NiS_4]$ unit

Atom	N [c]	Distance/Å	Range/Å
Ni(1)	1	0.04 (0.01)	0.03(1)–0.04(1)
Ni(2)	2	0.12 (0.10)	0.12(1)–0.12(1)
Ni(3)	2	0.07 (0.09)	0.06(1)–0.09(1)
Ni(4)	2	0.03 (0.07)	0.00(1)–0.06(1)
Ni(5)	2	0.06 (0.09)	0.05(1)–0.07(1)
Ni(6)	2	0.06 (0.03)	0.03(1)–0.08(1)

D. Sum of three angles about each S(i)

Atom	N [c]	$\Sigma_{S(i)}$/° [f]	Range/°
S(1)	4	299 (298)	290(1)–309(1)
S(3)	4	308 (313)	298(1)–313(1)
S(5)	4	298 (297)	288(1)–305(1)
S(7)	4	293 (295)	288(1)–304(1)
S(9)	4	309 (316)	299(1)–317(1)
S(11)	2	312 (297)	311(1)–312(1)

E. Ring sizes in **1** and **1a**

Distances	**1**	**1a**
Ni(1)–S(11)/S(12) [g]	11.545	10.712
Ni(4)–Ni(4′) [h]	11.706	12.388

[a] The means and individual ranges for symmetry-equivalent molecular parameters are for **1** in the triclinic crystal form; corresponding means for **1a** in the monoclinic crystal form are given in parentheses. [b] Atom-labeling, given in Fig. 1, is identical for the Ni–S toroids in **1** and **1a**. [c] N denotes the number of equivalent individual connectivities under pseudo-C_{2v} (2*mm*) symmetry; the principal two-fold axis, which passes through Ni(1) and the midpoint of S(11) and S(12), is crystallographically found in **1a**. [d] Av denotes the weighted average value. [e] δ is defined as the inner-ring dihedral angle between adjacent Ni(i)S_2 and S_2Ni(j) planes that intersect at the common S ··· S edge. [f] $\Sigma_{S(i)}$/° denotes the sum of the three bond angles around each S(i) atom; its value would be 360° for a trigonal planar S(i) and 328.5° for a regular tetrahedral S(i) (for which the unshared electron-pair and three connected atoms (*viz.*, the one R substituent and two Ni atoms) are assumed to conform to a regular tetrahedron (109.5°). In reality, the unshared electron-pair of a tetrahedral S(i) would have higher s-AO character than sp^3 hybrid and the bridging bonds and R substituent higher p-AO character resulting in a considerably smaller bond-angle sum than 328.5° (as observed). [g] Distance between the most separated Ni(1) and S(11)/S(12) (along the C_2 axis). [h] Distance between the most separated Ni(4) and Ni(4′) (perpendicular to the C_2 axis).

dihedral-angle description; each of the 11 dihedral angles, defined as the inner-ring angle between two adjacent $[NiS_4]$ planes that are edge-fused along a common nonbonding S ··· S edge, was calculated in **1** as the Ni–S_2(midpoint)-Ni angle, where S_2(midpoint) denotes the midpoint of the two edge-fused S atoms. These dihedral angles (denoted as δ) are observed in Table 1 to widely range from 113 to 213° in **1** on account of its 11-membered Ni–S ring possessing a combined *convex*/*concave*-like geometry corresponding to the inner ring δ values being *smaller*/*greater* than 180°, respectively. The smallest convex δ angle of 113° occurs for the two $[NiS_4]$ subunits that are edge-fused at S(11) and S(12) (Fig. 1).

Comparative analysis of mean molecular Ni–S ring parameters and the packing for triclinic 1 and monoclinic 1a

Fig. 3 presents the molecular configuration of *cyclo*-$[Ni(SPh)_2]_{11}$ (**1a**) in the monoclinic crystals. **1a** of pseudo-C_{2v} (2*mm*) symmetry lies on a crystallographic C_2 (2) axis. Its salient feature is that the entire geometry including the orientations of the phenyl rings is remarkably analogous to that of **1**.

The mean molecular Ni–S ring parameters for **1** and **1a** are presented in Table 1. All average values of corresponding values for distances between adjacent atoms in both **1** and **1a** are statistically equivalent, while some dihedral angles in **1a** slightly more deviate from the corresponding values in **1**. Overall, **1a** is compressed by ~0.8 Å along the C_2 symmetry axis of the molecule compared to **1**, which resulted in its expansion by ~0.7 Å in the direction, perpendicular to the C_2 axis (Table 1E). It is apparent that the observed polymorphism for $[Ni(SPh)_2]_{11}$ is dictated by packing effects that depend upon the number of solvated molecules.

To compare the packing of $[Ni_{11}(SPh)_{22}]$ rings in **1** and **1a**, each ring in the packing diagram was represented by a sphere centered in the geometrical center of the $Ni_{11}S_{22}$ ring. Both the triclinic and monoclinic lattices can be viewed as composed of layers of $Ni_{11}S_{22}$ rings, stacked along the z direction of the lattice, where each ring within the layer is inclined with respect

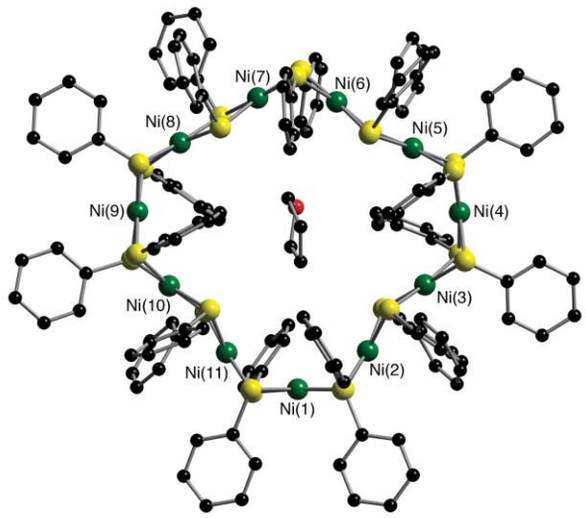

Fig. 2 Top view of the entire crystallographically independent neutral $[Ni(\mu_2\text{-}SPh)_2]_{11}$ (**1**) in the triclinic crystal form together with the co-crystallized solvated THF guest residing within its toroidal cavity. This guest C_4H_8O molecule, denoted by the red oxygen atom (that was not crystallographically distinguished from the other four ring C atoms), is aligned approximately along one vertical mirror and essentially bisected by the other mirror (containing the 11 Ni atoms) under assumed C_{2v} symmetry for the nickel–sulfur toroid. Inclusion of the phenyl substituents (with their spatial orientations), which for clarity are designated with circular carbon atoms, destroys the two pseudo-mirrors but roughly retains the pseudo-twofold axis. An analysis of the molecular parameters indicates no specific host–guest interactions in accordance with weak attractive dispersion forces. Hydrogen atoms and a crystal-disordered phenyl ring are omitted for clarity.

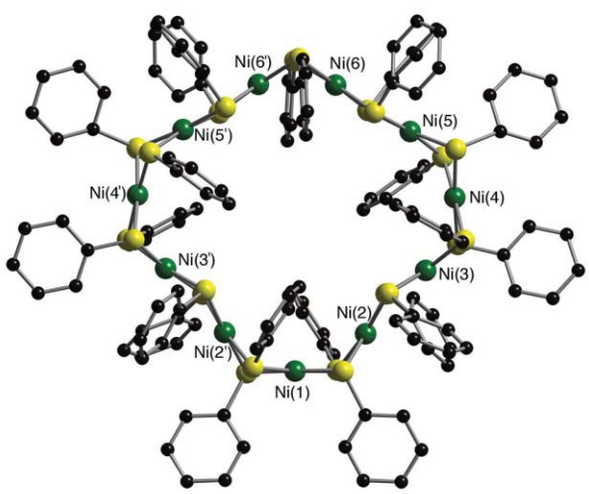

Fig. 3 Top view of the pseudo-C_{2v} $[Ni(\mu_2\text{-}SPh)_2]_{11}$ (**1a**) in the monoclinic form. This neutral molecule (**1a**) has crystallographic C_2 (2) site symmetry with the 2-fold axis passing through Ni(1) and the midpoint of S(11) and S(11′) such that one half of **1a** is crystallographically independent. Its entire molecular configuration including the spatial dispositions of the phenyl rings compares favorably with the molecular configuration of **1** in the triclinic crystal form (Fig. 2). Hydrogen atoms, crystal-disordered phenyl rings, and the THF molecule inside the cavity are omitted for clarity. Since the disorder originates from each phenyl ring being slightly rotated about its S–C bond, it does not significantly affect the position of the S–Ph vector with respect to the three parallel $S_{11}/Ni_{11}/S_{11}$ rings.

to the layer's plane. In **1** and **1a**, the angles of tilt are 24 and 62°, respectively.

[100], [010], and [001] projections of **1** and **1a** packing are shown in Fig. 4. An analysis of the packing diagrams discloses that the lattice of **1a** can be transformed into that of **1** by a compression of ~1.84 Å (*ca.* 13.2%) along the *z* direction with concomitant shift of every other layer along both the *x* and *y* directions and small increases in distances between $Ni_{11}S_{22}$ rings in every layer along the same directions. This transformation most likely originates from the presence of different number of solvated molecules in the crystal structures of **1** and **1a**.

Table 2 Mean molecular parameters under pseudo-D_{3h} symmetry of the Ni–S architecture in *cyclo*-$[Ni(SPh)_2]_9$ (**2**)

A. Bonding and non-bonding distances

Connectivity[a]	N[b]	Mean/Å	Range/Å
Ni(1)–S(1)	12	2.208	2.199(1)–2.218(1)
Ni(2)–S(1)	12	2.202	2.192(1)–2.212(1)
Ni(2)–S(3)	12	2.198	2.191(1)–2.204(1)
		Av[c] 2.203	
Ni(1) ··· Ni(2)	6	2.866(1)	
Ni(2) ··· Ni(2′)	3	3.239(1)	
		Av[c] 3.05	
S(1) ··· S(2)	6	2.925(1)	
S(3) ··· S(3′)	3	2.899(1)	
		Av[c] 2.91	
S(1) ··· S(1′)	6	3.31(3.29)	
S(1) ··· S(3)	12	3.32(3.27)	
		Av[c] 3.32(3.28)	

B. Dihedral angles

δ/°[d]	N[b]	Mean/°
$Ni(1)S_2Ni(2)$	6	121
$Ni(2)S_2Ni(2')$	3	203

C. Perpendicular displacement of Ni(*i*) from its mean sulfur plane in each $[NiS_4]$ unit

Atom	N[b]	Distance/Å
Ni(1)	3	0.05
Ni(2)	6	0.14

D. Sum of three angles about each S(*i*)

Atom	N[b]	$\Sigma_{S(i)}$/°[e]
S(1)	6	299
S(2)	6	307
S(3)	6	313

[a] Atom-labeling for the Ni–S toroid **2**. [b] N denotes the number of equivalent individual connectivities under pseudo-D_{3h} ($\bar{6}2m$) symmetry; [c] Av denotes the weighted average value. [d] δ is defined as the inner-ring dihedral angle between adjacent $Ni(i)S_2$ and $S_2Ni(j)$ planes that intersect at the common S ··· S edge. [e] $\Sigma_{S(i)}$/° denotes the sum of the three bond angles around each S(*i*) atom.

Structural features of the Ni–S architecture in the trigonal crystal form of *cyclo*-$[Ni(SPh)_2]_9$ (2)

The $Ni_9(\mu_2\text{-}S)_{18}$ framework and molecular configuration of **2** are given in Figs. 5 and 6, respectively, and its relevant molecular parameters are presented in Table 2. The crystallographically asymmetric part of **2** under crystallographic $D_3(32)$ site symmetry is comprised of two independent Ni atoms (of which one lies on one of the three horizontal 2-fold axes), three independent S atoms, and three independent phenyl groups. Its nickel–sulfur framework of pseudo-D_{3h} ($\bar{6}2m$) symmetry may be viewed as having a markedly deformed *convex*/*concave*-like "three-leaf" toroidal geometry; inclusion of the phenyl

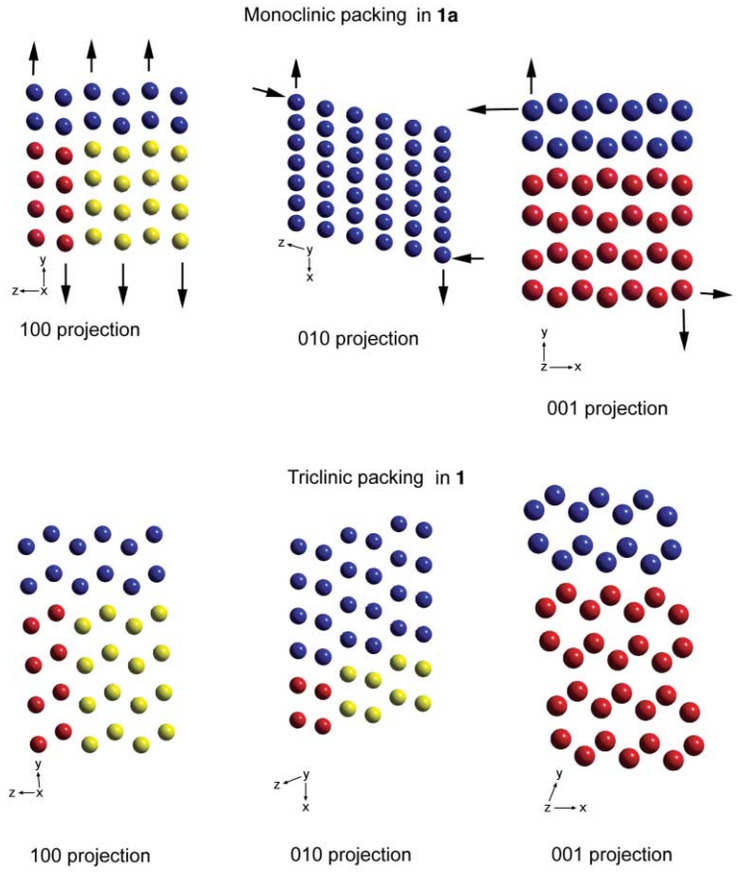

Fig. 4 Schematic representation of three major projections [100], [010], and [001] in the packing of **1** and **1a**, where the center of each $Ni_{11}S_{22}$ ring is represented by a sphere. Arrows on the packing projections of **1a** indicate the directions of hypothetical distortions in order to transform the monoclinic packing of **1a** into the triclinic packing of **1**. Colors are given to clarify the orientation of one projection relative to another. These relatively small but nevertheless distinct crystal-packing variations giving rise to two crystal forms of **1** (triclinic) and **1a** (monoclinic) are attributed to the dissimilar solid-state arrangements of the different numbers of solvated molecules.

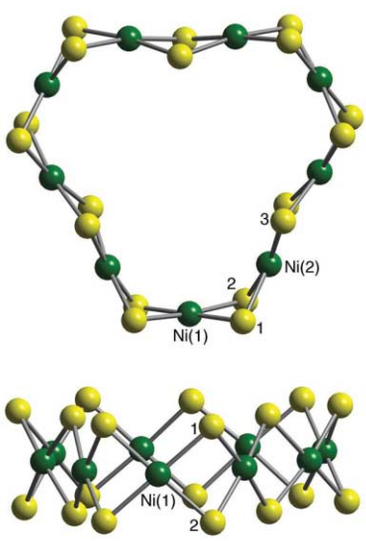

Fig. 5 Top and side views of the nickel–sulfur framework in $[Ni(\mu_2\text{-}SPh)_2]_9$ (**2**) which possesses crystallographic D_3 (32) site symmetry. The top view ideally shows that edge-fusion of the 9 localized planar $[NiS_4]$ subunits along opposite nonbonding S–S edges gives rise to a highly irregular convex/concave-shaped triple-layer toroidal geometry that approximately conforms to pseudo-D_{3h} symmetry.

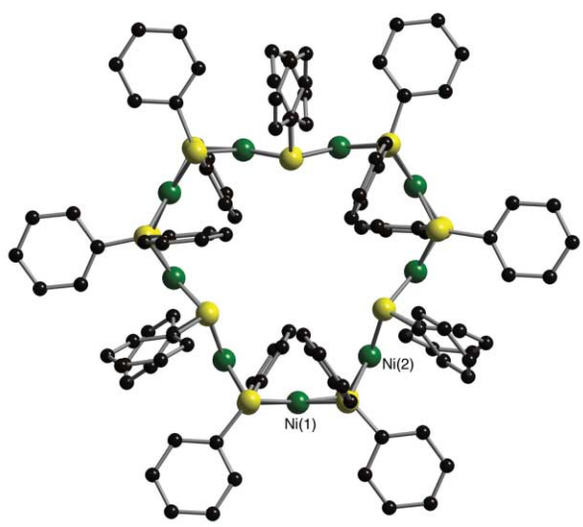

Fig. 6 Top view of the entire neutral $[Ni(\mu_2\text{-}SPh)_2]_9$ (**2**) which has crystallographic D_3 (32) site symmetry. The ring geometries of the bottom five edge-sharing $[NiS_4]$ subunits and steric dispositions of their sulfur-attached phenyl rings in **1** and **2** are closely analogous to each other (*i.e.*, compare this figure with Fig. 2).

substituents lowers the symmetry to the crystallographically imposed D_3 (32). Its cyclic molecular Ni–S framework is likewise ideally formed by edge-fusions of nine square-planar $[NiS_4]$ building blocks at opposite nonbonding S ··· S edges. Whereas the Ni(1) atom of the $[NiS_4]$ subunit (at the bottom of Figs. 5 and 6), through which one crystallographically horizontal twofold axis passes, is nearly coplanar (*i.e.*, Ni(1) is displaced from the mean of the four connected S atoms by 0.05 Å), the $[NiS_4]$ subunit containing the other independent Ni atom of general C_1 site symmetry is more deformed from a localized square-planar arrangement (*i.e.*, this Ni(2) atom is displaced by 0.14 Å from the mean plane of the four linked sulfur atoms). The close conformity of the entire Ni_9S_{18} fragment to D_{3h} symmetry is evident by the average deviation of the

Table 3 Mean molecular parameters for $[Ni(SPh)_2]_{11}$ and other $[Ni(SR)_2]_n$ toroids (n = 4, 5, 6, 8) with monodentate thiolate ligands

$[Ni(SR)_2]_n$	Ni–Ni/Å	Ni–S/Å	θ_1/° [a] S–Ni–S	θ_2/° [a] S–Ni–S	ϕ/° [a] Ni–S–Ni	Ref.
n = 4						
R = C_5H_9NMe	2.67	2.21	81	98	74	[d]
R = C_6H_{11}	2.69	2.21	81	98	75	[e]
R = *i*-Pr	2.68	2.21	81	98	75	[f]
n = 5						
R = Et	2.82	2.20	82	98	80	[g]
R = $(CH_2)_2N(i\text{-}Pr)_2$	2.79	2.18	82	98	80	[h]
R = CH_2SiMe_3	2.83	2.21	82	98	80	[i]
n = 6						
R = Me	2.91	2.21	82	98	83	[j]
R = Et	2.92	2.20	82	97	83	[k]
R = *n*-Pr	2.92	2.20	82	98	83	[m,n]
R = $(CH_2)_2OH$	2.92	2.21	83	98	83	[o]
R = $(CH_2)_2SiMe_3$	2.92	2.20	82	100	84	[p]
R = $CH_2C_6H_4$(*p*-Cl)	2.92	2.20	82	98	83	[q]
R = $(CH_2)_3NMe_2$	2.92	2.19	82	98	84	[r]
R = $(CH_2)_3NMe_2H^+$	2.93	2.20	82	98	84	[s]
n = 8						
R = CH_2CO_2Et	3.05	2.19	82	98	88	[t]
n = 9						
R = Ph	3.05	2.20	83	97	81,95	[u]
n = 11						
R = Ph	3.08	2.21	83 [b]	98	82 (Gp1) [c] 94 (Gp2) [c]	[u]

[a] θ_1 and ϕ denote interior intracyclic S–Ni–S and Ni–S–Ni bond angles, respectively, of Ni_2S_2 rings; θ_2 denotes an exterior Ni–S–Ni bond angle that is intercyclic to the Ni_2S_2 rings. [b] The θ_1(S–Ni–S) bond angles are closely distributed in **1** (mean, 83° without two outliers) except for the θ_1(S9–Ni5–S10) and θ_1(S9–Ni6–S10) angles of 77.5 and 77.6° involving the mirror-containing S9, S10 atoms formed at the apex by the edge-fusion of the two nearly linear mirror-related [–$S_2NiS_2NiS_2$–] fragments. [c] The two angles for each pair of ϕ(Ni–S–Ni) angles that are mirror-related by the pseudo-mirror containing the Ni atoms are close to another; however, there are two definite groups of ϕ(Ni–S–Ni) angles: Group 1 (mean, 82°) consisting of 14 angles for two face-fused convex-ring NiS_4 subunits and Group 2 (mean, 98°) consisting of eight angles for two face-fused concave-ring NiS_4 subunits. [d] Ref. 12. [e] Ref. 13. [f] Ref. 14. [g] Ref. 13. [h] Ref. 15. [i] Ref. 16. [j] Ref. 4. [k] Ref. 4b. [l] Ref. 2. [m] Ref 3. [n] Ref. 5. [o] Ref. 6. [p] Ref. 7. [q] Ref. 8. [r] Ref. 9. [s] Ref. 10. [t] Ref. 17. [u] This work.

nine nickel atoms from the mean pseudo-σ_h mirror plane being only 0.02 Å. Each of the three pseudo-σ_v mirror planes contains one Ni and two bridging S atoms. The principal crystallographic threefold axis is directed along the line of intersection of these three vertical pseudo-mirror planes.

Under crystallographic 32 site symmetry, the two independent dihedral angles (δ_1 and δ_2) were calculated to be 121 and 203°. The large difference between these two inner-ring angles denotes that the toroidal ring in **2** likewise has a highly deformed *convex*/*concave*-like geometry.[22]

Comparative analysis of the mean molecular nickel–sulfur ring parameters for 1 and 2 with those of the other $[Ni(\mu_2\text{-}SPh)_2]_n$ oligomers (n = 4, 5, 6, and 8)

Table 3 provides a geometrical comparison of the mean nickel–sulfur molecular parameters of **1**, **1a**, and **2** with those of the other $[Ni(\mu_2\text{-}SPh)_2]_n$ toroids (n = 4, 5, 6, and 8) with monodentate thiolate ligands. This table reveals the overall idealized geometrical conformity of the members within each of the n = 4, 5, and 6 polygonal systems.[23] For **1** and **1a**, the mean Ni–S bond length of 2.21 Å and mean θ_1(S–Ni–S) and θ_2(S–Ni–S) bond angles (defined in Table 3) of 83 and 98°, respectively, are virtually identical with those for all of the smaller size toroids.[24] The same is true for **2**, where the mean Ni–S bond is 2.20 Å long and mean θ_1(S–Ni–S) and θ_2(S–Ni–S) bond angles are 83 and 97°, respectively. In particular, the essentially invariant Ni–S bond lengths signify the major influence of the strong Ni–S bonds on the molecular geometries. A formal expansion in the size of the toroidal n-polygon from n = 4 to n = 8 results in systematic average enlargement of only the nonbonding Ni ··· Ni distances from 2.7 to 3.1 Å, respectively, and the ϕ(Ni–S–Ni) bond angles from 74 to 88°, respectively. The mean of 3.08 Å for the nonbonding Ni ··· Ni distances (range 2.86–3.42 Å) in **1** and the mean of 3.05 Å for the nonbonding Ni ··· Ni distances (range 2.87–3.24 Å) in **2** are analogous with that of 3.05 Å in the octagonal $[Ni(SCH_2COOEt)_2]_8$. However, the ϕ(Ni–S–Ni) bond angles in **1** were found to bunch around two different means of 82 and 94° (see footnote in Table 1). The corresponding two ϕ(Ni–S–Ni) bond angles in **2** also have values of 81 and 95°, almost identical with the corresponding mean values in **1**. The marked dissimilarity of these two means arises because of the combined *convex*/*concave*-shaped toroidal Ni–S geometry of **1** and **2** which, in order to maintain a semi-regularity of the localized square-planar geometries of the individual $[NiS_4]$ subunits, results in distinct twist-like deformations of these subunits from idealized C_{2v} and D_{3h} symmetries of Ni–S architectures, respectively (*i.e.*, see Figs. 1 and 5). The averages of these two mean ϕ(Ni–S–Ni) bond angles in **1** and **2** are identical with the mean ϕ(Ni–S–Ni) bond angle of 88° observed in the octagonal $[Ni(SCH_2CO_2Et)_2]_8$.

Presence of co-crystallized solvated guest within the host cavity of $[Ni(SPh)_2]_{11}$ in 1 and 1a but not within the smaller threefold-symmetrical cavity of $[Ni(SPh)_2]_9$ in 2

The triclinic crystal structure of $[Ni(\mu_2\text{-}SPh)_2]_{11}$ (**1**) presents the first definitive solid-state evidence for the co-crystallization of a guest molecule within its central cavity (Fig. 2). An initial electron-density difference map revealed that the electron-density peaks in this cavity are well approximated by atomic peaks of a single solvated C_4H_8O molecule. Four other crystal-

lographically independent solvated C_4H_8O molecules that occupy intermolecular cavities were similarly located in the triclinic unit cell. A notable structural feature of the THF molecule within the four-leaf clover-shaped $Ni_{11}S_{22}$ cavity (Fig. 1) is that its longest molecular dimension is roughly parallel to one of the two largest cavity diameters of 11.5 Å (Fig. 2). The C_4H_8O molecule is roughly bisected by the approximately planar undecamer of nickel atoms.

In the structurally analogous **1a** molecule, the encapsulated THF molecule is crystallographically disordered between two orientations related by the crystallographic 2-fold axis. Other solvated THF molecules that lie in intermolecular cavities were also found in the monoclinic unit cell, corresponding to an idealized formulation of $[Ni(SPh)_2]_{11}\cdot 6C_4H_8O$ for the monoclinic crystal form (**1a**).

In complete contrast, Fourier electron-density difference maps of the well-refined crystal structure of **2** conclusively showed the absence of any solvated guest molecule within its cavity. The nonpresence of a guest THF molecule is not at all surprising in light of the significantly smaller size of the symmetrically-shaped guest cavity in **2** coupled with the orientations of the bulky phenyl substituents that effectively prevent the occupation of an asymmetrically-shaped molecule with the van der Waals size dimensions of THF. Triclinic crystals of **1** were originally obtained from the dropwise addition of PhSH to $[Au_{16}Ni_{24}(CO)_{40}]^{4-}$ in DMSO; THF was subsequently used to extract the resulting dark brown solid, from which **1** was crystallized by a layering of the THF solution with *i*-Pr_2O. However, in subsequent direct preparations of **1**, **1a**, and **2** by addition of PhSNa to $Ni(ClO_4)_2$, reactions were performed either in DMSO or in THF. Consequently, it is presumed that Me_2SO may likely have been the initial solvated guest molecule facilitating the formation of **1** in its original preparation and that upon extraction the Me_2SO guest was then replaced with THF (*vide infra*).

Steric disposition of the phenyl rings in 1 and 2 and resulting implications concerning their formation

(a) ***Cyclo*-[Ni(SPh)$_2$]$_{11}$ (1).** An examination (Figs. 2 and 7) shows that the phenyl substituents in **1** adopt three different orientations with respect to the three parallel $S_{11}/Ni_{11}/S_{11}$ rings: *Axial* (*Ax*), for which the S–Ph vector is close to being perpendicular to the three rings; *Intermediate* (*Inter*), for which the S–Ph vector is inclined by 45–60° to the three rings; and *Equatorial* (*Eq*), for which the S–Ph vector is close to being parallel to the three rings. The resulting phenyl arrangement in **1** can be designated by two *clockwise* 11-membered cyclic sequences that are based upon the ring origin being chosen at S(11) and S(12), which are the only two sulfur atoms lying on one of the two pseudo-vertical mirror planes. These cyclic sequences are:

Above the Ni_{11}ring : *Ax(at S(11)) –Inter –Eq –Ax –Inter –Eq –Ax –Inter –Eq –Ax –Inter.*
Below the Ni_{11} ring: *Ax(at S(12)) –Inter –Ax –Eq –Inter –Ax –Eq –Inter –Ax –Eq –Inter.*

There are three complete common *Ax*-*Inter*-*Eq* phenyl conformations within each sequence with the fourth one lacking the last *Eq* conformation due to the 11-membered ring system, which disrupts the periodic cyclic conformational trend.

This scheme shows that no two S-attached Ph substituents that are related through the Ni_{11} mirror plane, can both have *equatorial* conformations due to steric repulsions. For the same reason, no two Ph substituents attached to adjacent S atoms within the same S_{11} ring can likewise have the same conformation. However, phenyl ··· phenyl π-stacking interactions may occur between *axially* and *intermediately* arranged adjacent phenyl rings in **1** and **2** (*vide infra*), because the adjacent phenyl rings in *Ax* and *Inter* conformations are nearly parallel (but offset) with each other (*i.e.*, angles between adjacent Ph rings in *Ax* and *Inter* conformations are in the range of 10–15°) and staggered with distances between the planes of these rings being in the range of 3.3–3.6 Å.

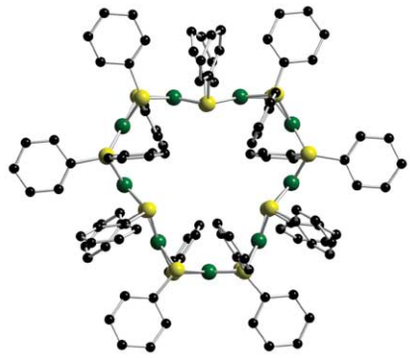

[Ni(SPh)$_2$]$_9$ (**2**)

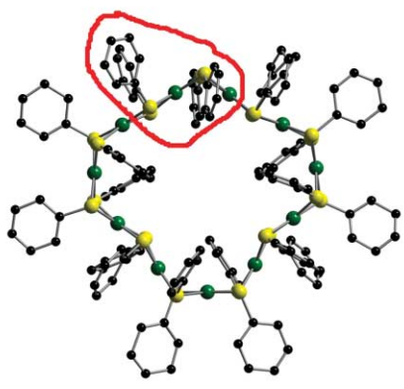

[Ni(SPh)$_2$]$_{11}$ (**1**)

Fig. 7 Top views of the entire molecular structures of **1** and **2** showing remarkable similarity in the Ni–S framework arrangement of these structures as well as in the conformations of the S-attached phenyl substituents. Red highlight denotes the additional two adjacent $[Ni(SPh)_2]$ units in **1** that are not present in **2**.

(b) ***Cyclo*-[Ni(SPh)$_2$]$_9$ (2).** Phenyl substituents in **2** similarly adopt two clockwise cyclic sequences of conformations with respect to the three parallel $S_9/Ni_9/S_9$ rings: based upon the origin being at two sulfur atoms lying on one of the three pseudo-vertical mirror planes, these cyclic sequences are:

Above the Ni_9 ring: *Inter(at S(3)) –Eq –Ax –Inter –Eq –Ax –Inter –Eq –Ax.*
Below the Ni_9 ring: *Inter(at S(3')) –Ax –Eq –Inter –Ax –Eq –Inter –Ax –Eq.*

In this case, three complete common *Ax*-*Inter*-*Eq* phenyl conformations follow one another in the 9-membered ring with no disruption in the periodic conformational trend.

(c) Comparison between 1 and 2. A comparison of the molecular structures of **1** and **2** in Fig. 7 (and especially the conformations of the phenyl substituents) reveals a striking similarity between the entire molecular geometry of **2** and the corresponding $Ni_9(SPh)_{18}$ fragment of the 11-membered $Ni_{11}(SPh)_{22}$ ring-geometry of **1**. The same sequence of conformations of the nine phenyl substituents in the geometry of the $Ni_9(SPh)_{18}$ fragment with those of **2** shows that **1** can be formally created from **2** *via* the formal edge-fused insertion of two adjacent $[Ni(SPh)_2]$ units into one leaf of the symmetrical three-leaf clover-shaped ring geometry of **2**.

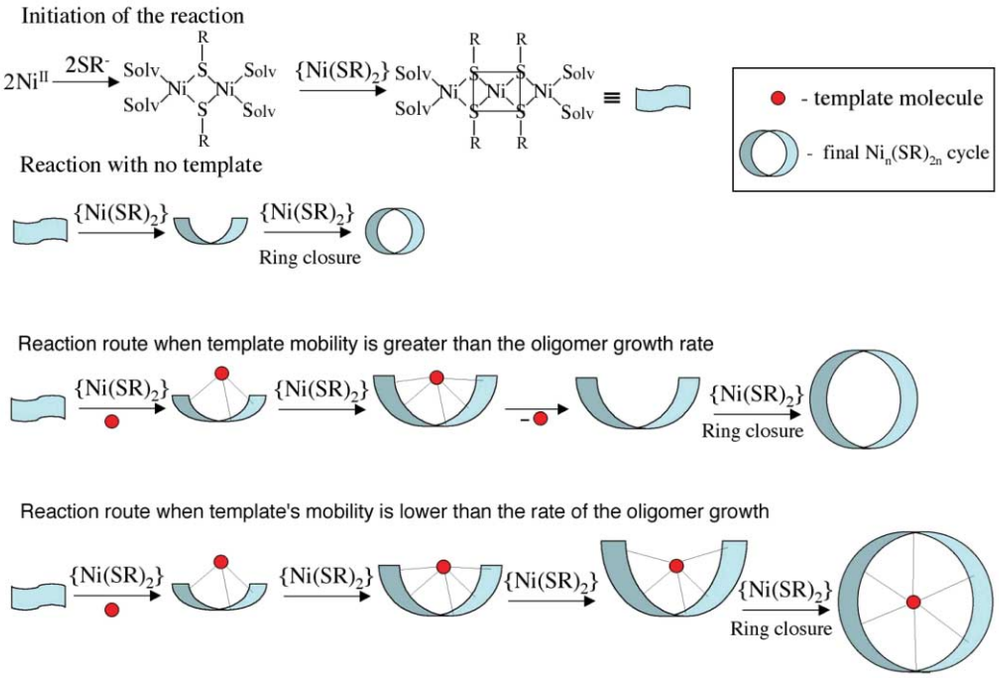

Fig. 8 Schematical representation of proposed different reaction pathways, which rationalize the dependence of size of $[Ni(SR)_2]_n$ ring on reaction conditions.

This close structural similarity between **1** and **2** indirectly suggests a common growth-pathway for these two oligomers, where the preference of one oligomer over the other one would appear to be determined primarily by the rate of ring-assembly and the relative mobility of a solvated template molecule to escape from the cavity.

(d) Postulated common growth-pathway for 1 and 2. A common synthetic growth-pattern is proposed in Fig. 8 for the creating of **1** and **2**. Our model is consistent with the original suggestion by Dance *et al.*[17] that the formation of larger toroids than the octagonal member ($n = 8$) is unlikely unless there is a central occupant (*i.e.*, either a guest molecule or reentrant ligand similar to the one observed for $n = 8$) that provides so-called "mechanical assistance". In other words, the unsymmetrical enlargement of the 11-membered ring cavity of **1** from the threefold-symmetrical 9-membered ring cavity if **2** is presumed to occur in order to accommodate an unsymmetrical template guest molecule.

Initial formation of both rings presumably involves the build-up of a one-dimensional oligomer of $L_2Ni[(SPh)_2Ni(SPh)_2]_n$-$NiL_2$ subunits (where L denotes terminal [PhS]/solvent ligation), where the length n is controlled by the reaction conditions and interactions of R substituents. Once the opposite ends of this "ribbon" meet, they would close the ring by forming two Ni–S bonds with simultaneous expulsion of two L ligands. If an unsymmetrical template molecule such as THF or DMSO (*i.e.*, $(CH_3)_2SO$) is involved in the growth process of the oligomer, it may prevent the oligomer from closing the ring too soon because of steric effects, which subsequently would lead to the formation of a large cyclic system. The lower the mobility of the template molecule relative to the rate of the oligomer "ribbon" growth, the higher the probability of larger ring formation. Upon ring closure, a slowly dynamic (and sufficiently small) template molecule may be trapped within the ring because of the bulky sulfur-connected phenyl substituents, which presumably may hinder the solvated molecule from escaping. One way to control the mobility of the template molecule relative to the rate of oligomerization is *via* a "slow" *versus* "fast" addition of PhS^- to the Ni^{2+} reactant. A lowering of the temperature would decrease the template mobility as well as the oligomer growth rate and thereby should favor the formation of a larger ring size. Another way to slow down the oligomer-growth rate is to decrease the number of growth centers by decreasing the concentration of the $[Ni(SPh)_2]$ building blocks, which in turn can be controlled by the decrease in concentration of phenylthiolate. We believe that the elongated molecular shape of the template molecule gives rise to the Ni_{11} ring system, which is stabilized by the π-interactions of the phenyl rings (*vide infra*). The proposed route is consistent with the formation of the 11-membered ring in **1** with an encapsulated THF or DMSO molecule *via* the "slow" addition of thiolate to the Ni^{2+} reactant at low temperature; in contrast, formation of the 9-membered ring in **2** should preferentially occur during the "fast" addition of thiolate to the nickel salt at room temperature. The smaller cavity size in **2** prevents the inclusion of a THF molecule.

An extended investigation revealed from X-ray crystallographic analysis that slow addition of the reactants in DMF (*i.e.*, $HC(O)NMe_2$) at −45 °C followed by recrystallization from THF solution afforded the THF-encapsulated $Ni_{11}S_{22}$ ring system in both the THF-solvated triclinic (**1**) and monoclinic (**1a**) crystal forms. The greater size of the DMF molecule suggests that a larger unsymmetrical template molecule (or a fragment thereof) is *not* necessarily encapsulated by the cyclic $Ni_{11}S_{22}$ system but leaves before formation of the ring geometry is completed. This strongly implies that the absence of an encapsulated guest molecule in **1** or **1a** would not affect its geometrical stability. The THF molecule then becomes a "guest" upon recrystallization.

Proposed attractive pairwise intramolecular phenyl ring interactions to account for the existence of the geometrically unprecedented two nickel(II) phenylthiolate oligomers, 1 and 2

The isolation of **1** as a unique undecagonal Ni–S toroid suggests that its highly unusual composition and resulting four-leaf clover-shaped geometry are consequences of the particular molecular dimensions of the solvated guest molecule and the maximization of attractive intramolecular dispersion forces between the phenyl substituents. The observed orientation of each sulfur-attached phenyl ring in **1** and **2** relative to those of neighboring phenyl rings points to the probable occurrence of van der Waals attractive, pairwise intramolecular phenyl-

··· phenyl interactions (*viz.*, offset face-to-face ones). The important role of aromatic π–π interactions in geometrically stabilizing other relatively small molecules as well as large biological systems is well-known.[25] Similar interactions in solid-state structures containing various $[PPh_3R]^+$ (R = Ph, Me) and $[AsPh_4]^+$ cations have been elegantly analyzed by Dance and coworkers[26] from quantitative energetic considerations.

A qualitative examination indicates that any bonding interactions between the $[Ni(SPh)_2]_{11}$ host and the co-crystallized THF guest would also be due to weak attractive dispersion forces.

Experimental

All reactions and manipulations were carried out under an atmosphere of air, unless stated otherwise, *via* standard Schlenk techniques. All solvents were dried and distilled under nitrogen prior to use. The following drying agents were used: THF (K/benzophenone), diisopropyl ether (molecular sieves), MeOH (Mg). PhSNa and $Ni(ClO_4)_2$ were purchased from Aldrich and used without further purification.

Several unsuccessful endeavors were made to ascertain the stoichiometries of **1** and **2** by use of the MALDI-TOF technique; however, no isotopic distribution patterns of the parent ions or of recognizable fragments were observed.

Synthesis and isolation of triclinic (1)/monoclinic (1a) crystal forms of *cyclo*-$[Ni(SPh)_2]_{11}$ and trigonal crystal form (2) of *cyclo*-$[Ni(SPh)_2]_9$

(a) Original preparation and isolation of 1. PhSH (0.15 ml, 170 eq.) in Me_2SO (15 mL) was added dropwise over 10 min to $[NMe_3Ph]_4[[Au_{16}Ni_{24}(CO)_{40}]$ (0.05 g) in Me_2SO (20 mL) under N_2 atmosphere. The solution lost its distinctive green–brown color after 10 min and became red-brown. After the solution was stirred for 24 h, successive additions of H_2O (initially 40 mL, then 100 mL) to the red–brown solution resulted in the precipitation of a dark brown solid, which was filtered, dried, and then extracted with THF. An IR solution spectrum of THF extract showed no bands characteristic of either carbonyl frequencies or S-H frequencies. A UV spectrum revealed a λ_{max} of 450 nm. Layering of this extract with *i*-Pr_2O gave a small quantity of black, block-shaped triclinic crystals (estimated yield, 2–4% based on Ni), what was characterized from the structural determination to be **1**. A considerable fraction of the solid obtained from the filtrate was insoluble in THF after drying.

(b) Subsequent preparation and isolation of 1 and 1a. PhSNa (0.20 g, 1.5 mmol) in THF (50 mL) was added dropwise under N_2 over one h. to a stirred solution of $Ni(ClO_4)_2$ (0.36 g, 1.0 mmol) in THF (20 mL) at 0 °C. Upon addition of PhSNa, the color of the mixture changed from light green to dark brown–red along with the formation of a brown residue. After removal of the THF by evaporation, the solid was twice washed with MeOH (20 mL). The solid first was extracted with THF, and the remaining residue was then separated from the THF solution by filtration. Layering of this THF extract with *i*-Pr_2O gave mostly block-shaped crystals along with some plate-shaped crystals (estimated yield of 20–30% based on Ni). Single-crystal X-ray diffraction measurements of the block-shaped crystals conclusively established that the triclinic lattice parameters agreed with those originally determined for **1**, and consequently further X-ray analysis has not been performed; a structural determination of the plate-shaped crystals revealed a monoclinic crystalline phase of **1**.

(c) Preparation and isolation of $[Ni(\mu_2\text{-}SPh)]_9$ (2). The reaction procedure for obtaining **2** by the reaction of PhSNa with $Ni(ClO_4)_2$ in THF solution is analogous to that which afforded the desired product, **1**. In fact, the reaction conditions (given above) that were used to isolate **1** along with **1a** were appropriately modified on the basis of the initial reaction having given rise to **2** instead of **1**. Major differences involved the rate of PhSNa addition, and the temperature of the reaction. A THF solution of PhSNa was added relatively quickly to $Ni(ClO_4)_2$ in THF at room temperature. The resulting dark red–brown solid was also washed with MeOH, and then extracted with THF. A layering of the THF solution with n-hexane produced thick plate-shaped crystals, from which a single-crystal X-ray diffraction study unambiguously established both the atomic arrangement and composition of **2** (estimated yield was 20–30% based on Ni).

X-Ray diffraction analyses

(a) General comments. Crystallographic data are given for the triclinic and monoclinic crystal forms, **1** and **1a**, respectively, of *cyclo*-$[Ni(SPh)_2]_{11}$ and for the trigonal crystal form of *cyclo*-$[Ni(SPh)_2]_9$ (**2**). A black rhombic-shaped crystal of dimensions 0.12 × 0.08 × 0.06 mm for **1**, a black thick plate-shaped crystal of dimensions 0.40 × 0.20 × 0.10 mm for **2**, and a black plate-shaped crystal of dimensions 0.3 × 0.05 × 0.2 mm for **1a** were used for data collection. Intensity data were collected at −100 °C *via* a Bruker SMART CCD area-detector system mounted on a Bruker Platform diffractometer with graphite-monochromated Mo-Kα radiation (λ = 0.71073 Å) from a standard sealed-tube generator. An empirical absorption correction (SADABS) was applied to each data set. Structural determinations were obtained by use of direct methods followed by successive Fourier difference maps. Least-square refinements (based on F^2) were performed with SHELXTL.[27] Ideal hydrogen atoms, initially determined geometrically, were refined by a riding model.

(b) Crystal structure analysis of 1. $[Ni(SC_6H_5)_2]_{11}\cdot 5C_4H_8O$, M = 3407.85, triclinic, $P\bar{1}$, Z = 2, a = 17.535(2) Å, b = 19.518(2) Å, c = 24.994(3) Å, α = 82.095(2)°, β = 75.406(2)°, γ = 72.380(2)°, V = 7872.5(15) Å^3, ρ_{calcd} = 1.438 Mg m^{-3}. A sphere of 34311 data was collected *via* 0.3° ψ scans (120 s per frame) over a 2θ 3.2–45.0°; [μ[MoKα] = 1.625 mm^{-1}; max./min. transmissions, 0.909/0.829]. **1** has crystallographic C_1(1) site symmetry such that the entire molecule is crystallographically independent. Five co-crystallized solvated THF molecules were located from difference Fourier maps, of which one C_4H_8O molecule was found to be a guest within the host cavity. Anisotropic refinement (1276 parameters/57 restraints) on 20483 independent merged data (R_{inter} = 0.141) converged at $wR_2(F^2)$ = 0.27 for all data; $R_1(F)$ = 0.092 for 7053 observed data ($I>2\sigma(I)$). This refinement was based upon the following boundary conditions: (1) One of the 22 independent phenyl rings is equally distributed over two independent crystallographic sites (*i.e.*, the occupancy factor α for each of the 12 site positions was determined to be approximately 0.5); (2) Twelve of the 132 phenyl carbon atoms including the 12 half-weighted carbon sites of the one crystal-disordered phenyl ring were refined isotropically in order to avoid the occurrence of non-positive-definite temperature-displacement parameters; and (3) Nonhydrogen atoms of the five solvate THF molecules were refined isotropically; each THF molecule was modeled as five C ring atoms in that the oxygen atom could not be unambiguously assigned. The final difference map, which had max./min. residual density of 1.07/−0.67 e Å^{-3}, showed no abnormal features. Mean molecular parameters of Ni–S framework are presented in Table 1.

(c) Crystal structure analysis of 1a. $[Ni(SC_6H_5)_2]_{11}.xC_4H_8O$, M = 3479.97 (x = 6), monoclinic, $C2/c$, Z = 4, a = 18.888(2) Å, b = 29.401(4) Å, c = 28.354(4) Å, α = 90°, β = 98.995(4)°, γ = 90°, V = 15552(3) Å^3, ρ_{calcd} = 1.336 Mg m^{-3}. A sphere of 60,554 data was collected *via* 0.3° ψ scans (60 s per frame) over a 2θ range of

2.6–56.6°; [μ[MoKα] = 1.64 mm^{-1}; max./min. transmissions, 0.697/0.510]. **1a** has crystallographic $C_2(2)$ site symmetry corresponding to one-half of the molecule being crystallographically independent. The unit cell of $C2/c$ symmetry contains four $[Ni(SPh)_2]_{11}$ oligomers and ideally 24 solvated THF molecules: namely, four twofold-disordered $Ni_{11}S_{22}$-encapsulated THFs, four other THFs that also are disordered on crystallographic $C_2(2)$ sites, and 16 THFs that occupy two sets of 8-fold general positions. The anisotropic least-squares refinement (825 parameters/60 restraints) on 18453 independent merged data (R_{int} = 0.054) converged at $wR_2(F^2)$ = 0.192 for all data, $R_1(F)$ = 0.059 for 18453 observed data ($I > 2\sigma(I)$). This refinement was based upon the following boundary conditions: (1) Of the 11 independent phenyl rings, six are each equally disordered *via* two independent crystallographic sites. All full-weighted and half-weighted carbon sites were refined anisotropically; (2) The nonhydrogen atoms in each THF molecule were modeled as five carbon atoms (in that the oxygen atom could not be readily identified) and refined isotropically. The eight crystal-disordered THF molecules each lying on a twofold axis were modeled with the twofold axis passing through two of the five ring atoms. The abnormally large isotropic thermal parameters of some of the ring atoms may be a consequence of partial crystal occupancies as well as unusually large atomic displacements from their equilibrium positions.

Due to refinement instability, two THF molecules were refined without assigned hydrogen atoms at idealized positions. The largest positive residual densities (max., 1.37 e Å^{-3}) in the final electron-density difference map were attributed to incompletely modeled density from crystallographically disordered THF molecules positioned outside the host ring. Mean molecular parameters of the Ni–S framework are presented in Table 1.

(d) Crystal structure analysis of 2. $[Ni(SC_6H_5)_2]_9$·(x solvated molecules), M = 2493.3 (for **2** only), trigonal, $P\bar{3}12/c$, Z = 2, $a = b$ = 18.024(1) Å, c = 21.118(2) Å, $\alpha = \beta$ = 90°,γ = 120°, V = 5941.2(7) Å^3, ρ_{calcd} = 1.474 Mg m^{-3} (for **2** only). A sphere of 36387 data was collected *via* 0.3° ψ scans (20 s per frame) over a 2θ range of 2.6–52.7° [μ[MoKα] = 1.756 mm^{-1} (for **2** only) max./min. transmissions, 0.844/0.541]. **2** has crystallographic $D_3(32)$ site symmetry such that 1/6 of one molecule is crystallographically independent. All nonhydrogen atoms were refined with anisotropic displacement coefficients. Anisotropic refinement (211 parameters/0 restraints) on 4340 independent merged data (R_{inter} = 0.075) converged at $wR_2(F^2)$ = 0.098 for all data; $R_1(F)$ = 0.037 for 4054 observed data ($I>2\sigma(I)$). Six of the 18 phenyl rings are equally disordered over two crystallographic sites. Fourier difference maps showed no evidence (*i.e.*, no residual electron density) for a solvated guest molecule within the cavity of *cyclo*-$[Ni(SPh)_2]_9$ in accordance with its cavity size being sterically too small to accommodate either a THF or hexane molecule; however, they provided definitive evidence for the existence of solvated molecules (presumed to be THF) at two large *intermolecular* centrosymmetric-related cavities of crystallographic $D_3(32)$ symmetry at 0 0 1/4; 0 0 3/4 for the entire hexagonal unit cell. Attempts to interpret the composite electron density within one crystallographic independent cavity in terms of crystal-disordered solvated molecules were unsuccessful. The final difference map had max./min. residual densities of 0.37/−0.24 e Å^{-3}. Option SQUEEZE of program PLATON[28] was used to correct the diffraction data for diffuse scattering effects at the two cavity sites. This program estimated the upper limit of volume for both cavities that can be occupied by the solvent to be 412.0 Å^3, or 6.9% of the unit cell volume. Because the resulting volume of each cavity is 206 Å^3, an assumed average volume of 19 Å^3 per nonhydrogen atom (observed in other high-nuclearity metal carbonyl clusters) gives 206 Å^3/19 Å^3 = 11.8 (*i.e.*, 12) nonhydrogen atoms for each of the two cavities. This suggests that each cavity would contain either one or a maximum of two solvated THF (*i.e.*, C_4H_8O) molecules that are highly disordered due to the crystallographic $D_3(32)$ site symmetry. PLATON gave an estimated total electron count of 63 electrons for each cavity that is consistent with the probable formulation of one crystal-disordered solvated THF (*i.e.*, 72 electrons per molecule) at each cavity site. After corrections for the independent crystal-disordered solvated molecule, the final least-square refinement on 4340 independent merged data (R_{inter} = 0.075) converged at $wR_2(F^2)$ = 0.096 for all data; $R_1(F)$ = 0.037 for 4340 observed data ($I>2\sigma(I)$). The final difference map, which now had max./min. residual density of 0.385/−0.261 e Å^{-3}, was featureless. However, all calculated results in the supplementary tables are based only on the $[Ni(SPh)_2]_9$ molecules (*i.e.*, without contributions from the crystal-disordered solvated molecules). Mean molecular parameters of the Ni–S framework are presented in Table 2.

CCDC reference numbers 167795 for **1**, 186293 for **1a**, and 186294 for **2**.

See http://www.rsc.org/suppdata/dt/b2/b204273h/ for crystallographic data in CIF format.

Acknowledgements

This research was supported by the National Science Foundation (CHE-9729555). The CCD area-detector diffractometry system was purchased in part in 1995 with an NSF grant (CHE-9310428). We thank Dr. Ilia Guzei (UW-Madison) for helpful crystallographic advice. Color figures were prepared with Crystal Maker, Interactive Crystallography (version 5). David C. Palmer (P.O. Box 183 Bicester, Oxfordshire, UK OXG 7BS).

References and notes

1 (*a*) K.A. Jensen, *Z. Anorg. Chem.*, 1944, **252**, 227; (*b*) R. G. Hayter and F. S. Humiec, *J. Inorg. Nucl. Chem.*, 1964, **26**, 807.
2 (*a*) P. Woodward, L. F. Dahl, E. W. Abel and B. C. Crosse, *J. Am. Chem. Soc.*, 1965, **87**, 5251; (*b*) E. W. Abel and B. C. Crosse, *J. Chem. Soc.*, 1966, 1377.
3 The original structure of $[Ni(\mu_2\text{-}SEt)_2]_6$ obtained for the monoclinic crystal form from X-ray photographic data[2] was subsequently redetermined more precisely by use of X-ray diffractometry data for both the monoclinic and triclinic crystal forms. H. Miyamae and T. Yamamura, *Acta Crystallogr., Sect. C*, 1988, **C44**, 606.
4 (*a*) T.A. Wark and D.W. Stephan, *Organometallics*, 1989, **8**, 2836; (*b*) K. Schulbert and R. Mattes, *Z. Naturforsch. B*, 1994, **49**, 770.
5 H. Feld, A. Leute, D. Rading, A. Benninghoven, G. Henkel, T. Krüger and B. Krebs, *Z. Naturforsch. B*, 1992, **47**, 929.
6 R. O. Gould and M. M. Harding, *J. Chem. Soc. A*, 1970, 875.
7 A. H. Mahmoudkhani and V. Langer, *Polyhedron*, 1999, **18**, 3407.
8 C. Jin-Hua and K. Bei-Sheng, *Chin. J. Struct. Chem. (Jiegou Huaxue)*, 1993, **12**, 397.
9 M. Capdevila, P. Ginzales-Duarte, J. Sola, C. Foces-Foces, F.H. Cano and M. Martinez-Ripoll, *Polyhedron*, 1989, **8**, 1253.
10 H. Barrera, J. C. Bayon, J. Suades, C. Germain and J. P. Declerq, *Polyhedron*, 1984, **3**, 969.
11 N. R. Kunchur, *Acta Crystallogr., Sect. B*, 1968, **B24**, 1623.
12 W. Gaete, J. Ros, X. Solans, M. Font-Altaba and J. L. Brianso, *Inorg. Chem.*, 1984, **23**, 39.
13 M. Kriege and G. Henkel, *Z. Naturforsch. B*, 1987, **42**, 1121.
14 T. Krüger, B. Krebs and G. Henkel, *Angew. Chem., Int. Ed. Engl.*, 1989, **28**, 61.
15 A. H. Mahmoudkhani and V. Langer, *Inorg. Chim. Acta*, 1999, **294**, 83.
16 B-K. Koo, E. Block, H. Kang, S. Liu and J. Zubieta, *Polyhedron*, 1988, **7**, 1397.
17 I. G. Dance, M. I. Scudder and R. Secomb, *Inorg. Chem.*, 1985, **24**, 1201.
18 A. Müller and G. Henkel, *Z. Naturforsch., B: Chem. Sci.*, 1997, **52**, 1501.
19 P. Alemany and R. Hoffmann, *J. Am. Chem. Soc.*, 1993, **115**, 8290.
20 Much work has been done to obtain monodispersed thiolate-monolayer-stabilized Au clusters in order to study their properties especially size-dependent quantum effects: (*a*) M. Brust, M. Walker, D. Bethell, D. J. Schiffrin and R. Whyman, *J. Chem. Soc., Chem.*

Commun., 1994, 801; (*b*) S. Chen, R. S. Ingram, M. J. Hostetler, J. J. Pietron, R. W. Murray, G. T. Schaaf, J. T. Khoury, M. M. Alvarez and R. L. Whetten, *Science*, 1998, **280**, 2098 and references therein; (*c*) L.O. Brown and J. E. Hutchison, *J. Am. Chem. Soc.*, 1997, **119**, 12384.

21 This 40-atom close-packed bimetallic pseudo-T_d nanocluster (metal-core diameter, 0.98 nm) possesses a microscopic ccp Au_{16} kernel that is stabilized by close-packed Au–Ni bonding with four tetrahedrally disposed triangular $[Ni_6(CO)_3(\mu_2\text{-}CO)_6(\mu_3\text{-}CO)]$ fragments (M. A. Kozee and L. F. Dahl, to be submitted for publication).

22 A triclinic crystal form of *cyclo*-$[Ni(SPh)_2]_9$ (**2a**) has been subsequently isolated and structurally analyzed. Of prime interest is that its entire molecular geometry including the phenyl-ring orientations is virtually identical with that described for **2** in its trigonal crystal form. Crystal data for triclinic form: a = 14.469 Å, b = 17.841 Å, c = 26.248 Å, α = 94.19°, β = 95.57°, γ = 105.57°, V = 6461.4 Å^3, $P\bar{1}$ Z = 2.

23 The different sterically demanding effects of the particular R substituents in each toroidal nickel–sulfur member coupled with crystal-packing forces are observed to cause considerable localized perturbations of the Ni–S frameworks from their idealized geometries in individual toroidal $[Ni(SR)_2]_n$ members. A prime example is $[Ni(S(CH_2)_2SiMe_3)_2]_6$ which has highly distorted $[NiS_4]$ subunits that are ascribed to the bulky R substituents.[4] The importance of crystal packing forces in causing molecular distortions is illustrated by the geometry of $[Ni(SMe)_2]_6$ being severely distorted in one crystal form[4a] but essentially undistorted in another crystal form.[4b].

24 On the basis of a mean Ni–S bond length of 2.21 Å and mean θ_1(S–Ni–S) and θ_2(S–Ni–S) bond angles of 83 and 98°, respectively, the calculated nonbonding mean S ··· S distances in an average undistorted rectangular NiS_4 subunit are 2.9 Å in height and 3.3 Å along each side.

25 (*a*) C. Janiak, *J. Chem. Soc., Dalton Trans.*, 2000, 3885 and references therein; (*b*) C. A. Hunter and J. K. M. Sanders, *J. Am. Chem. Soc*, 1990, **112**, 5525 and references therein; (*c*) C. A. Hunter, *Chem. Soc. Rev.*, 1994, **23**, 101 and references therein.

26 G. R. Lewis and I. Dance, *Inorg. Chim. Acta*, 2000, **306**, 160 and references therein.

27 All software and sources of the scattering factors are contained in the *SHELXTL (version 5.1) program library* (G. Sheldrick, *Bruker Analytical X-Ray Systems*, Madison, WI).

28 A. L. Spek, *Acta Crystallogr., Sect. A*, 1990, **A46**, C-34.